splaced by ψ_o and longitudinal dimensions decrease as ε (in the case of ellipsoidal bunches they decrease as $1 - S$). After some calculations we get

$$I = \frac{3{,}12\, E_m r_o^2 \varphi_s \sin \varphi_s}{\lambda M_z} \cdot \frac{\varepsilon (1 - \varepsilon + \psi_o/\psi_s)}{0.18}, \quad [16]$$

where $M_z = B_3 - B_2$. Taking into account that ψ_o/φ_s is small as compared to $1 - \varepsilon$, assuming $r_o^2 = R^2/\gamma$, $\tau = 1$, $\varepsilon = 1 - S$ and replacing $\varepsilon(1 - \varepsilon + \psi_o/\varphi_s)/M_z$ by its maximum value, Eq. [16] agrees with [1] except for 4% — difference in the coefficients.

In the case [12] with $R^2/\gamma = r_o^2$ and $\tau = 1$ one obtains $I_M = 127$ m A (and $S_M = 0.34$, $M_z = 0.222$) from Eq. [1] based on the ellipsoidal bunch approximation. The expression [16] on cylindrical (non self-consistent) approximation gives $I_M = 210$ m A (where $I - \varepsilon_M = 0.3$, $M_z = 0.130$), i.e. by 65% more. Note that in (3) obviously overestimated current $I_M = 0{,}6 \cdot I_o = 400$ mA was obtained for the same initial data. Electronic computation (3) was not carried out to $h_\varphi = 1$ (corresponding to $\varepsilon = 0$) but was arbitrarily extrapolated to this value. In the paper (3) the conclusions were made, that the maximum current value is attained at $h_\varphi = 1$ and phases stability region is slightly dependent on the self-charge effect. Due to the arbitrary extrapolation, mentioned above, these conclusions are ungrounded. Actually the phase stability region and therefore the particle current reduce to zero at $h_\varphi = 1$ ($\varepsilon = 0$).

4. CONCLUSION

The representation of accelerated bunches by uniformly charged ellipsoids used for obtaining the limit current expression is shown to be approximately self-consistent (sect. 2). Due to simplicity and computation advantages this approximation seems to be rather good. Expression [1] may be considered to be grounded enough being corroborated by experimental data.

The self-consistency problem solution is not the single one More or less probable arbitrary of the bunch charge distribution (sect. 2) or of the distribution on the phase plane (sect. 3) have been admitted in the very beginning. Even with these assumptions an infinite number of self-consistent distributions are possible as, for example, in sect. 2.

In conclusion note that the quite different initial assumptions adopted in (1, 2) and (3) lead to limit current expressions [1] and [16] which are quite analogous in character and slightly differ quantitatively.

REFERENCES

(1) A. D. Vlasov: NT-2460-33, Radiotechnical Institute, Academy of Sciences (1960).
(2) Linear Accelerator Theory and Design, pp. 94, 114 (Gosatomizdat, Moscow, 1962).
(3) I. M. Kapchinskij and A. S. Kronrod: Space Charge Effect in Particle Phase Oscillations in Ion Linear Accelerator. Int. Conf. on High Energy Accelerators, Dubna, 1963.
(4) A. D. Vlasov: Theory of Linear Accelerators (Atomizdat, Moscow, 1965).

DEVELOPMENT OF THE CROSS-BAR STRUCTURE FOR A PROTON LINEAR ACCELERATOR

A. Carne[1], G. Dôme, N. Fewell[2] and W. Jüngst[3]
CERN, Geneva, (Switzerland)

(Presented by G. Dôme)

1. INTRODUCTION

The cross-bar structure is being studied at CERN for an injector linac into a synchrotron. As such it must fulfil the usual requirements of high shunt impedance, and good mechanical and r.f. tolerances. These tolerances and the need of a good transient response for beam loading compensation all require a wide bandwidth. Such a large bandwidth is a major feature of the cross-bar structure, and full advantage of this is obtained by operating the structure in the reso-

[1] CERN, on leave from Rutherford Laboratory.
[2] Rutherford Laboratory.
[3] CERN, on leave from Technische Hochschule, Karlsruhe. Mr. Fewel and Dr. Jüngst were responsible for experimental measurements.

nant-coupled π-mode. It will be seen that, in terms of shunt impedance alone, the cross-bar structure is better than the Alvarez structure for energies greater than about 100 MeV, but the further requirements, and additionally the mechanical standardization that may be achieved, make the cross-bar strutcure distinctly better.

The basic principles and results of the field theory for the cross-bar structure are presented. Because of the rather complicated shape of the metallic boundaries, an exact theory for the actual structure is extremely complicated. Nevertheless it is possible to derive the main characteristics by considering, firstly, a rectangular waveguide periodically loaded with two alternating sets of bars at right angles (the two sets may have different diameters); secondly, a circular guide with bars but without drift tubes; thirdly, a circular guide with bars and drift tubes.

Semi-empirical formulae for drift tube capacitance and transit time factor are deduced. The characteristic equations so obtained are used to give a near-optimised structure over the energy range 80-300 MeV, which is compared with designs of the Alvarez structure.

2. SQUARE GUIDE WITHOUT DRIFT TUBES

The main features of a rectangular structure without drift tubes (see Fig. 1a) are easily derived from the basic assumption that the electromagnetic fields outside the bars may be computed as if the net currents flowing along them were concentrated on their axes (1); this assumption meaning essentially that the bars are thin enough to make the fields due to circumferential currents negligible or, quantitatively, that $(2\rho/L)^2 \ll 1$. This yields the dispersion diagram and the space harmonics of the fields along the waveguide axis for any mode.

In π-mode, the field configuration becomes particularly simple and reduces to that of TEM waves propagating along one set of parallel bars. Each bar may then be considered as the inner condcutor of a transmission line, the outer conductor being constituted by the waveguide walls which are parallel to the bar, and fictitious metallic walls in the cross-sectional planes containing the other set of bars (see Fig. 1b). The characteristic impedance Z_0 of this transmission line is related to the electromagnetic stored energy, and thus influences all other properties of the structure.

When TEM waves are propagating along one set of bars in π-mode, they are not perturbed by the other set (as far as the assumption $(2\rho/L)^2 \ll 1$ holds); a consequence, the resonant frequency is then determined essentially by the length of the former bars, which must be half a free space wavelength. In general therefore, there are two resonant frequencies in π-mode, each of them corresponding to one set of bars carrying a net longitudinal current. In terms of coupling, there is a mutual inductance between the two sets of bars, but, due to symmetry, its net effect is zero in π-mode. As soon as the phase shift per cell differs from π, the effect of coupling becomes apparent and, as with coupled resonators, two pass-bands are built up from the two (unperturbed) π-mode resonance frequencies.

When these two π-mode frequencies are made equal (to the degree of approximation used above, by making the bars of equal length, i.e. by making the waveguide square), the coupling becomes resonant, and the two pass-bands merge into a single one with the π-mode at the band centre. The group velocity now remains finite at that mode, taking the value

$$\left|\frac{v_g}{c}\right| = \frac{\left(\frac{\pi}{2}\frac{L}{D}\right)}{\operatorname{sh}\left(\frac{\pi}{2}\frac{L}{D}\right)} \operatorname{th}^2\left(\frac{\pi}{2}\frac{L}{D}\right) \cdot \sqrt{\frac{\cos\frac{\pi\rho_1}{D} - \cos\frac{\pi\rho_2}{D}}{\log\frac{L}{K\rho_1}\log\frac{L}{K\rho_2}}} \qquad [1]$$

where $D = a = b$ is the side of the square, and $K(k)$ is the complete elliptic integral of the first kind such that $K(\sqrt{1-k^2})/K(k) = b/L$.

Since the coupling constant is proportional to the group velocity at the centre of the pass-band, it is seen that the magnetic coupling constant and bandwidth increase from zero to large values with increashing radii ρ_1, ρ_2 of the bars. Nevertheless, this process is limited on the side of the 0-mode when the 0-mode frequency reaches the E_{11}-mode cut-off of the empty square guide (which corresponds to the E_{01}-mode cut-off for a circular guide). At that point, an increase of the bar diameters no longer increases the 0-mode frequency, and the widening of bandwidth is slowed down. However, for a structure with $\beta = 0.5$, the bandwidth then is already as large as 0.50 to 0.60.

When the structure is terminated by an end plate containing a bar, the net longitudinal current along that bar must be zero, and this boundary condition determines the standing wave pattern (2). In any mode, there is a longitudinal current flowing along all bars, except those bars whose phase difference with respect to the end-plates is a multiple of π. In particular, in π-mode, the currents vanish in the whole set of bars which terminates in the end-plates.

Fig. 2 * shows measured E- and H-field patterns for various modes in the cross-bar structure. In all modes different from π, a magnetic field exists around all barse (except those in the end-plates), but in π-mode it exists only around one set of bars. The figure justifies the concept of coupled coaxial resonators in the fundamental TEM mode used previously (3, 4) to synthesize modes in the cross-bar structure.

To the present degree of approximation, the π-mode resonance frequency of the first set of bars is determined only by their length. A further step takes into account the effect of the circumferential currents induced in the second set of bars by the TEM standing waves supported by the first set: these currents are equivalent to oscillating electric dipoles which have the effect of lowering the resonant frequency by an amount that is easily computed with Slater's perturbation formula, as

$$\frac{\delta\omega}{\omega} = -\left(\frac{2\rho_2}{L}\right)^2 \frac{1}{\log(L/K\rho_1)} \frac{\pi L}{2a} \left[1 - \frac{\pi b}{L} \frac{4\exp(-\pi b/L)}{1+2\exp(-\pi b/L)}\right] \qquad [2]$$

This formula has been compared with experiment. Although they are small, computed and measured frequency shifts agree to better than 9%, even when the formula is applied to circular guides with a = b = D. Measurements of the axial electric field have also been performed on S-band models, using a perturbing bead. They agree with the theoretical field to within 5%, as well for circular as for square guides without drift tubes.

As stated in the introduction, the cross-bar structure will be operated in resonant-coupled π-mode. Therefore, in what follows, interest is centered on this mode.

3. CIRCULAR GUIDE WITHOUT DRIFT TUBES (π-mode)

In the case of a circular guide, each bar may still be considered as the inner conductor of a

* This figure supercedes that in ref. 4.

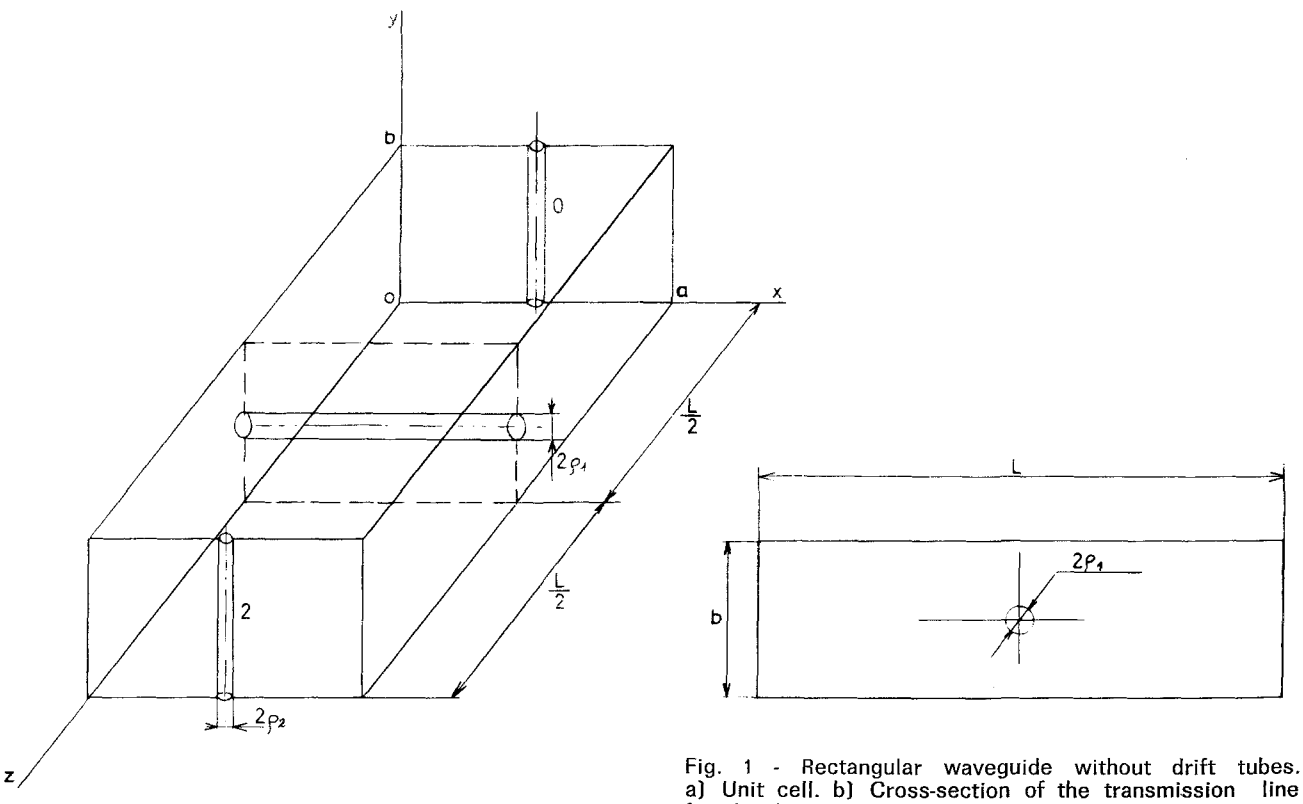

Fig. 1 - Rectangular waveguide without drift tubes. a) Unit cell. b) Cross-section of the transmission line for the first set of bars.

transmission line. But, since the guide wall which constitutes part of the outer conductor is no longer parallel to the bar, the transmission line is no longer uniform. Sitrctly speaking, the waves supported by this line are no longer TEM with respect to the bar. But, for the sake of simplicity, they are still considered as such waves propagating along a transmission line of variable characteristic impedance. This impedance is computed at each point along the bar from the (variable) plane cross-section of the line (see Fig. 3).

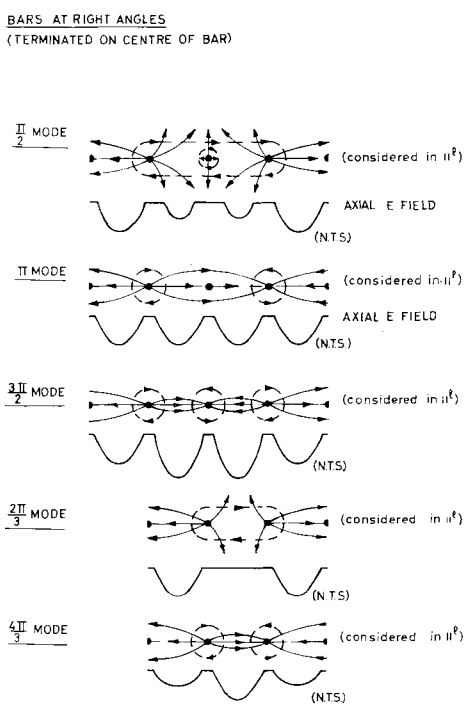

Fig. 2 - Field patterns for coupled coaxial resonators.

The differential equation for the current I along the bar is then

$$\frac{\partial^2 I}{\partial x^2} + \frac{d \log Z_o}{dx} \frac{\partial I}{\partial x} + \frac{\omega^2}{c^2} I = 0 \qquad [3]$$

where

$$Z_o \approx 60 \log \left\{ \left(\frac{4L}{\pi d_o}\right) - 2 \log \left[1 + 2 \exp\left(-\frac{\pi D}{L} \cdot \sqrt{1 - \left(\frac{2x}{D}\right)^2} \right) + 2 \exp\left(-4\pi \frac{D}{L} \sqrt{1 - \left(\frac{2x}{D}\right)^2} \right) + \ldots \right] \right\} \Omega$$

The characteristic impedance Z_o varies from a maximum value Z_{oo} at the centre of the bar, to zero at the point $x = r_s$ where the bar touches the guide wall (see Fig. 4). To obtain an analytical solution of equation [3], Z_o has been replaced by a simple function with similar shape, of the type $Z_{oo}(1 - x/r_o)^{\alpha}$, α being a small exponent which is adjusted to equalize the areas under both curves. As a result of this treatment a correction factor ζ (ranging between 0.95 and 1) appears in the characteristic equations of the cross-bar structure, summarized in Table I. For a rectangular guide this correction does not apply, and $\zeta = 1$.

The resonant frequencies thus calculated for circular structures loaded with one set of bars agree with experimental results to within 0.15%. When the structure contains two sets of bars, the frequency correction given by equation [2] must be added to the ζ-correction. As a net result, the two sets of bars have different π-mode resonant frequencies as soon as they have different diameters. To investigate this, a 900 MHz 20-cell model without drift tubes was made (5) with alternate bar diameters in the ratio 2:1. The π-mode frequencies were 893.1 MHz (thick bars) and 885.7 MHz (thin bars), and compare closely with the theoretical values 892.7 MHz and 883.1 MHz. At π-mode (see figure 5) the mean group velocity, disregarding the splitting, was 0.132 c, compared with 0.142 c theoretical.

On a 940 MHz, 140 MeV, model of the optimised structure described in section 5, π-mode (main bar) is at 943.2 MHz, and π-mode (thin bar) is 27.4 MHz lower. In that case, the different kinds of drift tubes contribute to increase the splitting. However, this splitting can easily be removed by use of tuners at the base of the thin bars: the tuners will increase the π-mode frequency of these bars and, to a much smaller extent, will decrease the π-mode frequency of the main bars. Alternatively, making the thin bars some 6 mm thicker will equalise the frequencies (the frequency tolerance at 200 MHz is about 0.9 MHz per mm change in stem diameter, and is roughly constant over the energy range). However, the base tuners will be retained for fine tuning, and general cavity tuning.

4. CIRCULAR GUIDE WITH DRIFT TUBES (π-mode)

Drift tubes are added to the bars in order to improve the transit time factor; at the same time, they may house magnetic quadrupoles for radial focusing.

a) Axial transit time factor (TTF)

Theoretical values of axial TTF for the cross-bar structure with drift tubes are not yet avai-

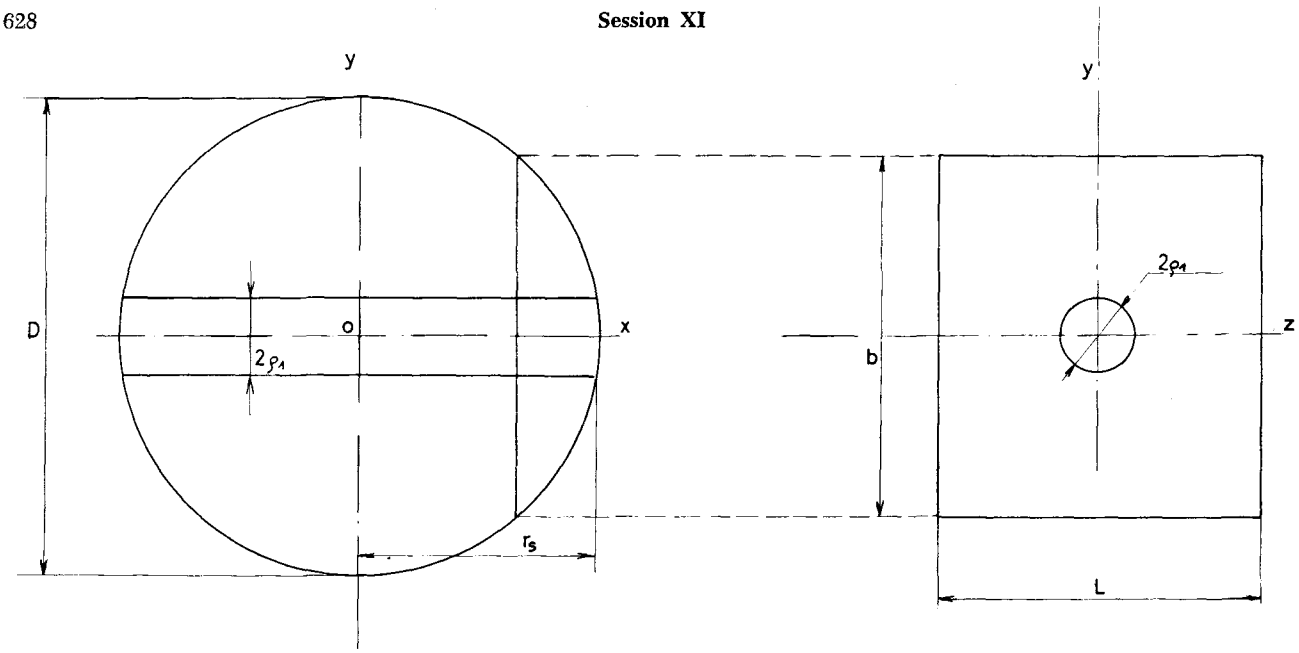

Fig. 3 - Circular waveguide without drift tubes. a) Cross-section through the first set of bars. b) Cross-section of the variable transmission line for the first set of bars.

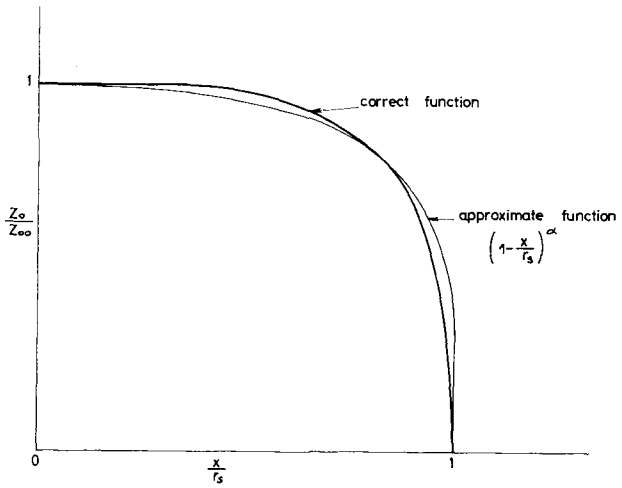

Fig. 4 - Variation of characteristic impedance along the bars.

lable because of the difficulty of describing accurately the axial field E (z). Nevertheless, good semi-empirical formulae can be obtained, based on Fourier analysis of simple π-mode E-field patterns. The first, and obvious, choice is to assume uniform fields in the gaps (4) (a fair assumption when the ratio 2g/d is not larger than unity). This gives

$$T_o = \sin\frac{\pi}{2L}(l_1 + g)\sin\left(\frac{\pi g}{2L}\right)\Big/\left(\frac{\pi g}{2L}\right) \qquad [4]$$

A discussion of this formula and its implications ca be found in ref. 4. It shows that for optimum TTF, the drift tubes on the current carrying bars must be rather long, while on the second set of bars they must be as short as possible. This leads to the arrangement of figure 6 (where all symbols can be found).

Comparison of formula [4] with experimental results (on models of constant drift tube diameter) gives agreement to 0.5% at beat and 5% at worst. The formula can be modified to fit experiment rather better by using

$$T \approx T_o\left[1 - \frac{1}{6}\left(\frac{\pi g}{2L}\right)^2\right] \approx \left(\frac{\pi g}{2L}\right)\cot\left(\frac{\pi g}{2L}\right)\sin\frac{\pi}{2L}(l_1 + g) \qquad [5]$$

On the same models, the error is now less than 2%. This formula has been used in section 5 when computing the "optimised" cross-bar structure.

Neither formula [4] nor [5] contains the drift tube diameter explicitly, and measurements are being made to study the dependency on d. Fig. 7 shows variations of TTF with d for square ended drift tubes and for two values of aperture (the frequency is maintained constant at 800 MHz by adjusting the gap length): it is seen that TTF reduces as d increases. Clearly, for the range of d considered in full scale (corresponding to 30, 32.5, 35 mm in model), and since the gaps must necessarily be even smallor to compensate the rounding of the drift tube corners, the use of formula [5] in the optimisation program is good to 2%.

b) Drift tube capacitance

The drift tubes are providing essentially capacitive loading to the transmission lines of the crossed bars. From the resonance condition (equation [8] in Table I), the effective experimental value 2C of this capacitance (C is the capacitance of one gap) has been reduced and compared with the value

$$2C_{isolated} = \left(\frac{d}{3} + \frac{l}{6}\right)\frac{1}{9.10^{11}} \text{ Farads} \qquad [6]$$

computed for an ellipsoid of same external dimensions (d, l) isolated in space (formula [6] is a good approximation when l/d remains in the neighbourhood of unity). A semi-empirical correction factor

$$\left[1 - \exp\left(-\frac{4}{\pi}\cdot\frac{2g}{d}\right)\right]$$

has been introduced to account for the finite size of the gap, but the most difficult correction is due to the prseence of the bars on the drift tubes. This has been roughly accounted for by replacing l bq ($l_t - d_s$) in formula [6].

Due to all these approximations the final formula for the capacitance of a drift tube, given by equation [7] in Table I, may be wrong by 20% when $d/\lambda = 0.12$ (what corresponds to quite a large drift tube), but the error does not exceed 10% when $d/\lambda \leqslant 0.08$.

In spite of these inaccuracies, the equations of Table I may be used to optimize the cross-bar structures for maximum shunt impedance, because this maximum appears to be extremely flat against small variations of the structure geometry (see section 5a).

c) Bandwith

It is easy to see that not only the π-mode but every mode is capacitively loaded by the drift tubes. Since the loading increases from the 0- to the 2π-mode, the bandwidth is larger than for a structure without drift tubes. Nevertheless the slope of the $\omega - \beta$ diagram at π-mode was found to be only slightly increased, so that equation [1], although derived for a square guide without drift tubes, may still be used to compute the group velocity in a circular guide with drift tubes, with an error less than 10%.

If one set of bars is removed, the passband extends only from 0 to π, and the coupling between the remaining parallel bars reduces to a small value due to the drift tubes and to the

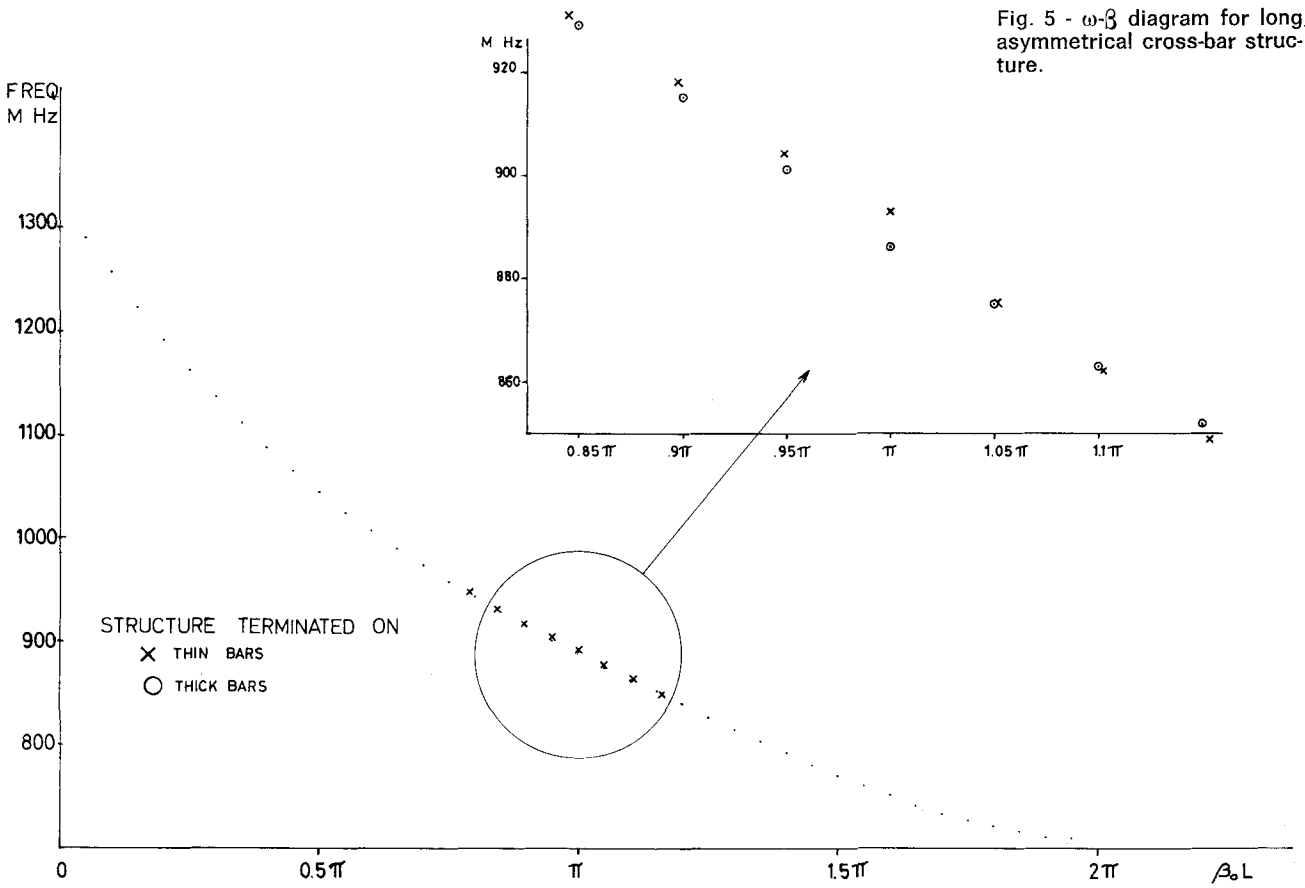

Fig. 5 - ω-β diagram for long asymmetrical cross-bar structure.

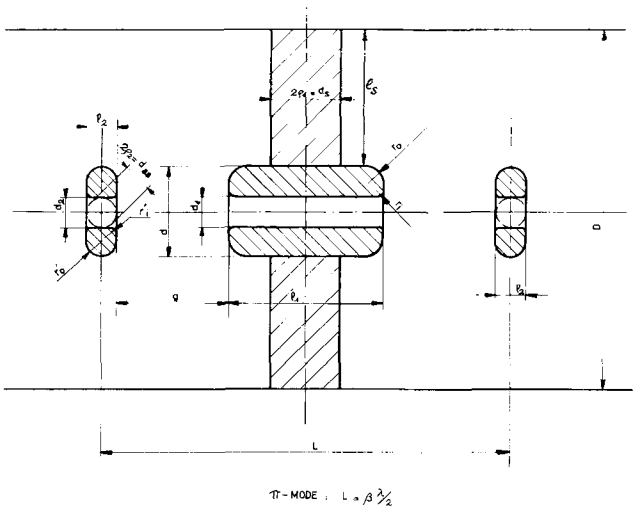

Fig. 6 - Unit cell of the cross-bar structure.

circular shape of the guide. Both effects act to reduce the bandwidth very much: in a typical case (5), it went from 0.73 down to 0.13.

5. OPTIMUM DIMENSIONS OF THE CROSS-BAR STRUCTURE

a) Computation of parameters

With the characteristic equations summarized in Table I, the variation of shunt impedancs Z_{eff} and Q-value has been determined as function of liner diameter D and thick bar diameter d_s for values of drift tube diameter d of 12, 13, 14 cm, with constant size small drift tube and support bar, $l_2 = d_{ss} = 3.81$ cm (1.5 inches). This has been done over the energy range 80-300 MeV, and at the chosen operating frequency 200 MHz. Fig. 8 shows the optimum (theoretical) shunt impedance against energy for the three drift tube diameters: variation with energy is slow, and with d is roughly 0.5 MΩ/m per cm change. A drift tube diameter of 12 cm is practicable from the points of view of r.f. breakdown capability (4), focusing and quadrupole technology: so this value is taken for the optimum structure. For optimum Z_{eff} over the energy range, D varies from 64 to 68 cm (D/L = 2.13 to 1.4), and d_s from 7 to 11.5 cm ($L/d_s = 4.3$ to 4.24). But variation of Z_{eff} with D and d_s was found to be so slow that, with an almost negligible increase in r.f. power loss, it is possible to have a constant liner diameter, D = 66 cm, throughout the energy range, and only two values of d_s : $d_s = 8$ cm for 80-150 MeV, $d_s = 10$ cm for 150-300 MeV $L/d_s = 3.65$-4.75; 3.80-4.89, respectively). In a system with so many components with constant dimensions the advantages both in cost and mechanical construction are clearly very great.

Q-values for the structure with these dimensions are shown in Fig. 9, and vary between 18,000 and 23,000 over the energy range. Low Q's lead to shorter build-up times and easy mechanical tolerances. On the other hand, it is well known [6, 7, 8, 9] that for reasons of phase shifts along an accelerator tank, mode separation, transient response and beam loading compensation, the best operating mode is a π/2 mode or, even better for its larger bandwidth, a resonant-coupled π-mode. The performances then depend essentially on the product of Q and bandwidth, which in the cross-bar structure has been measured (4) to be of the order of 0.80. Thus the large bandwidth more than compensates the low Q.

b) Comparison with experiment

Experimental tests have been made with several models: at 80, 200 MeV [4], 300 MeV, all at 800 MHz; and with S-band models without

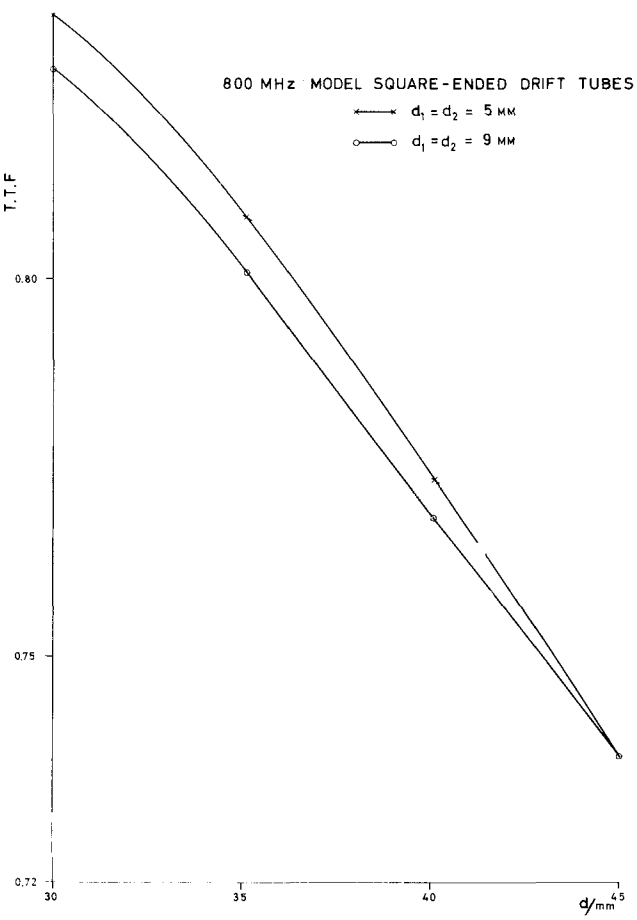

Fig. 7 - Transit time factor against drift tube diameter.

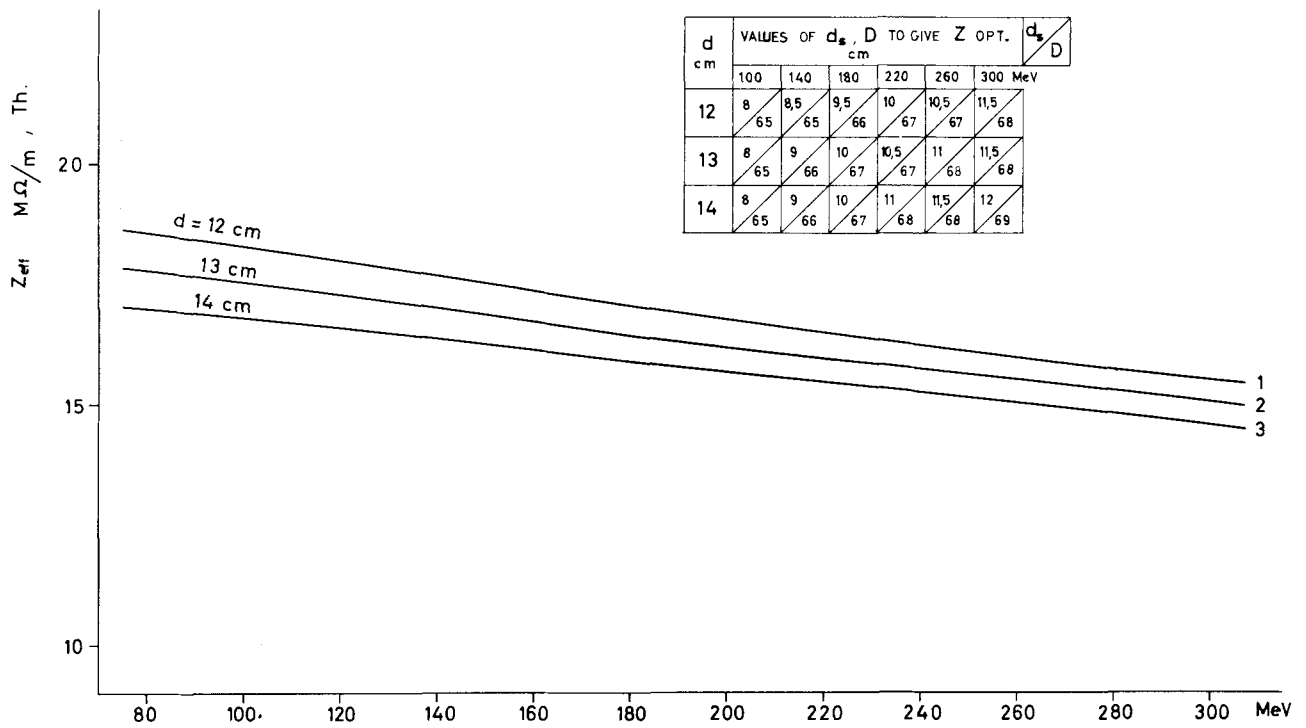

Fig. 8 - Optimum theoretical shunt impedance of cross-bar structure.

drift tubes (for which, as has been described, the theory is much simpler). In all drift tube models the experimental Z_{eff}/Q values were 10-20% higher than theoretical, the discrepancy being greater the smaller L/d_s (the models had $L/d_s = 6, 8, 10$). Q-values on S-band copper plated brass models (no drift tubes) at $\beta = 0.55, 1.0$ were respectively 92%, 94.5% of theoretical. An average ration of 2.08 was found for the Q's of copper and brass models. For 800 MHz soft-soldered brass models with drift tubes, Q's at $\beta = 0.4, 0.56$ were respectively 98%, 92% of theoretical, allowing a factor 2 between brass and copper. At 200 MHz, in copper and with properly brazed joints, Q's of the order of 95% of theoretical should be obtainable. The Z_{eff}/Q values are expected to be 15% (mean) greater than theoretical. But despite this discrepancy in absolute value of Z_{eff}/Q, the optimisation process is still considered a good one. This has been verified on a 940 MHz model of the structure in a) above for $L/d_s = 5.4, 4.13$ (the theoretical optimum), 3.2. The value of Z_{eff}/Q for $L/d_s = 4.13$ was indeed the maximum, and was 22.2% greater than theoretical.

c) Optimum structure and comparison with the Alvarez structure at 200 MHz

Fig. 10 compares the structure with dimensions labelled in a) with two designs of Alvarez structure: a MURA design for the proposed ANL 200 MeV injector (10), and a 200 MeV linac for CERN (11). The cross-bar structure now includes a 15% increase in shunt impedance in accordance with b) above. The Alvarez linacs include 20% "non-theoretical" losses (those on stems and end-plates contribute about 15% of total loss), but that this is enough is questioned. The cross-bar structure is seen to have a shunt impedance larger than the Alvarez linac for energies greater than about 100 MeV, and gives a 30% saving in r.f. power at the

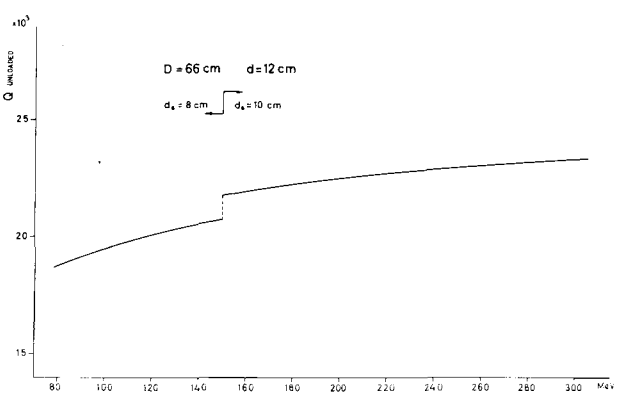

Fig. 9 - Unloaded Q of optimised cross-bar structure.

TABLE I

Characteristic equations of the cross-bar structure

$$r_s = \frac{D}{2}\sqrt{1-\left(\frac{d_s}{D}\right)^2}\,; \quad l_s = r_s - \frac{d}{2} \qquad [1]$$

$$\frac{2K}{\pi} = \left[1 + 2\exp\left(-\pi\frac{D}{L}\right) + 2\exp\left(-4\pi\frac{D}{L}\right) + \ldots\right]^2 \qquad [2]$$

$$Z_c = 60\log\left(\frac{2}{K}\frac{L}{d_s}\right) = 60\log\frac{L}{K\rho_1}\ \text{ohms} \qquad [3]$$

$$J\left(\frac{L}{D}\right) = 2\int_0^1 du\cdot\log\left[1 + 2\exp\left(-\pi\frac{D}{L}\sqrt{1-u^2}\right) + 2\exp\left(-4\pi\frac{D}{L}\sqrt{1-u^2}\right) + \ldots\right] - \log\frac{2K}{\pi} \qquad [4]$$

$$\varepsilon = \left[J\left(\frac{L}{D}\right) - 0.1292\left(\frac{d_s}{D}\right)^2\right] \Big/ \log\left(\frac{2}{K}\frac{L}{d_s}\right) \qquad [5]$$

$$\zeta = \left[\frac{1-\varepsilon}{\sqrt{1-\left(\frac{d_s}{D}\right)^2}}\right]^{0.500000 + 0.131111\left(\pi\frac{l_s}{\lambda}\right)^2 + 0.065185\left(\pi\frac{l_s}{\lambda}\right)^4} \qquad [6]$$

$$2C = \frac{\frac{d}{3} + \frac{l_1 - d_s}{6}}{1 - \exp\left(-\frac{4}{\pi}\cdot\frac{2g}{d}\right)}\cdot\frac{1}{9\cdot 10^{11}} \qquad [7]$$

C, capacitance of one gap in Farads
all lengths in cm

$$(\zeta k l_s)\cdot\operatorname{tg}(\zeta k l_s) = \frac{l_s}{c\,Z_0\,C};\ k = \frac{2\pi}{\lambda} \qquad [8]$$

$$T = \left(\frac{\pi g}{2L}\right)\operatorname{cotg}\left(\frac{\pi g}{2L}\right)\cdot\sin\frac{\pi}{2L}(l_1 + g) \qquad [9]$$

$$Q_o = 13104.6\,\beta\sqrt{\lambda}\,\frac{d_s}{L}\log\left(\frac{2}{K}\frac{L}{d_s}\right)(1-\varepsilon);\ \lambda \text{ in cm} \qquad [10]$$

$$\frac{Q_c}{Q_\infty} = 1 + \pi\left(\frac{d_s}{L}\right)\zeta\beta\cdot\frac{\log\left(\frac{2}{K}\frac{L}{d_s}\right)}{\zeta k l_s + \sin(\zeta k l_s)\cdot\cos(\zeta k l_s)} + \pi\left(\frac{d_s}{L}\right)\cdot\frac{4\exp\left(-\pi\frac{D}{L}\right)}{1 + 2\exp\left(-\pi\frac{D}{L}\right)} \qquad [11]$$

$$\frac{Q_o}{Q_{1\,\text{cell}}} = \frac{Q_o}{Q_\infty} + \frac{d_s}{L}\left[1 - \pi\frac{D}{L}\cdot\frac{4\exp\left(-\pi\frac{D}{L}\right)}{1 + 2\exp\left(-\pi\frac{D}{L}\right)}\right] \qquad [12]$$

$$Z_{\text{eff}} = \frac{Q_\infty}{1-\varepsilon}\,T^2\,8\,\frac{Z_o}{L}\,\frac{\zeta^3\sin^2(\zeta k l_s)}{(\zeta k l_s) + \sin(\zeta k l_s)\cdot\cos(\zeta k l_s)} \qquad [13]$$

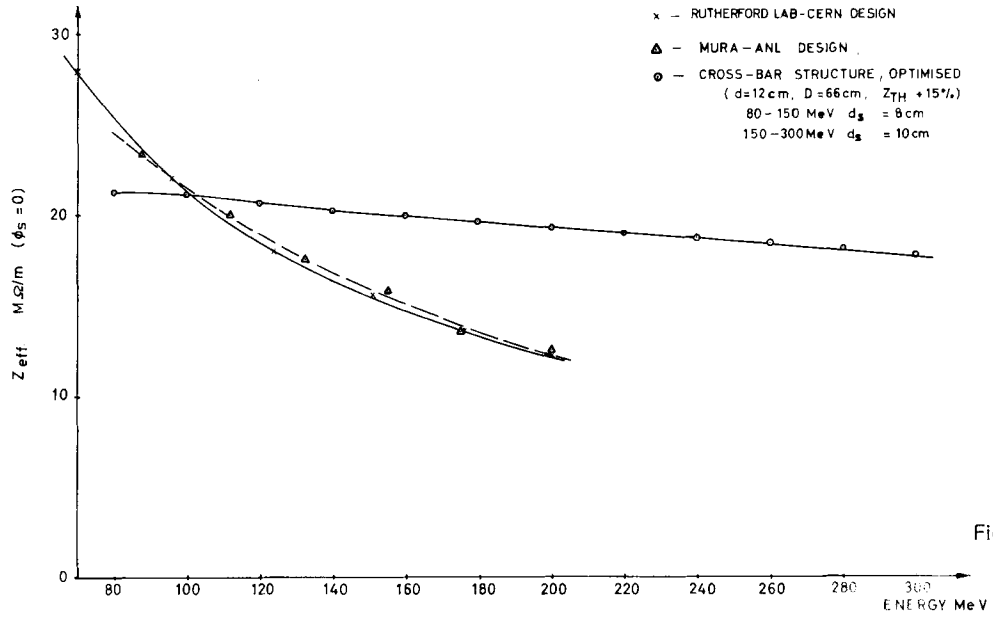

Fig 10 - Cross-bar and Alvarez structure shunt impedances.

quoted acceleration rates for the same energy range (100-200 MeV). To this advantage can be added: the possibility of mechanical standardization, a low Q and a wide bandwidth (or high group velocity in π-mode), and since the structure has a 20% smaller surface area, a corresponding reduction in the cost of vacuum equipment.

Acknowledgement

We wish to thank Dr. Pierre Lapostolle for many stimulating discussions.

REFERENCES

(1) G. Dôme: A theoretical investigation of the cross-bar structure, CERN Report AR/SG, (1964).
(2) G. Dôme: Comparison of shunt impedances near the π-mode for symmetrical and asymmetrical structures, CERN Report AR/SG, (1964).
(3) A. Carne: Proc. Yale Conference on Linacs, (1963).
(4) A. Carne: Proc. 1964 Linac Conference, MURA 714, (1964) p. 1.
(5) A. Carne and N. M. Fewel: P.L.A. Progress Report 1964, NIRL/R/81, (1964), p. 20.
(6) J. H. Adlam and P. D. Dunn: Notes on coupled pill box resonators operating in π-mode, AERE Report GP/R 1539, (1954).
(7) P. D. Dunn, C. S. Sabel and D. J. Thompson: Coupling of resonant cavities by resonant coupling devices, AERE Report GP/R 1966 (1956).
(8) E. Knapp: 800 MeV r.f. structures, 1964 Linear accelerator conference, MURA Report 714, p. 55.
(9) H. G. Hereward and P. Lapostolle: Energy flow and transients in the Alvarez structure, CERN Report AR/Int. SG/65-12 (1965); Paper presented to this Conference, see Appendix.
(10) Lee Teng et al.: Proposal for an Improvement Program for the ZGS, ANL Report, (1964).
(11) A. Carne and K. Batchelor: Design of a high current 200 MeV proton linear accelerator, NIRL/R/55 (1964).